Sensors and Actuators B 235 (2016) 627–635

Contents lists available at ScienceDirect

Sensors and Actuators B: Chemical

journal homepage: www.elsevier.com/locate/snb

Responsivity of the differential-intensity surface plasmon resonance instrument

Sidahmed A. Abayzeed[a,b,*], Richard J. Smith[a,b], Kevin F. Webb[a,b], Michael G. Somekh[c], Chung W. See[a]

[a] Advanced Optics Group, Faculty of Engineering, University of Nottingham, Nottingham, NG7 2RD, UK
[b] Institute of Biophysics, Imaging and Optical Science (IBIOS), University of Nottingham, Nottingham, NG7 2RD, UK
[c] Electronic and Information Engineering, The Hong Kong Polytechnic University, Hung Hom, Kowloon, Hong Kong, China

ARTICLE INFO

Article history:
Received 8 December 2015
Received in revised form 5 May 2016
Accepted 24 May 2016
Available online 24 May 2016

Keywords:
Surface plasmon resonance
Bi-cell surface plasmon resonance system
Biosensing
Chemical sensing

ABSTRACT

Surface plasmon resonance is used for the sensitive measurement of minute concentrations of bio-analytes and probing of electrochemical processes. Typical refractive index sensitivity, for the intensity approach, is around 10^{-6} refractive index units (RIUs). A better sensitivity has been suggested by developing a differential-intensity detection method. This method relies on the excitation of surface plasmons using a weakly focused beam with the average angle of incidence equal to the resonance angle, while the reflected light is detected using a bi-cell photodiode. The Bi-cell signal is processed by calculating the difference between its two units, normalized to their sum. This ratio estimates the shift in the resonance angle using a model that represents the resonance curve with a quadratic function. However, this model does not explain the effects of parameters such as the angular width of the excitation beam and the specifications of the sensing structure on the system's response. This paper presents a detailed evaluation of the responsivity using experimental and theoretical approaches, which can predict the effect of the different parameters, paving the way towards the investigation of a better sensitivity and the optimization of the system's design for different applications.

1. Introduction

Surface plasmon resonance (SPR) sensors are powerful analytical tools that are capable of detecting small concentrations of analytes, providing a wide range of medical and scientific applications [1]. This sensing technique relies on the excitation of longitudinal surface plasmon oscillations at the metal-dielectric interface by directing p-polarized light of a matching spatial frequency on the surface of the metal. The excitation beam is coupled to the interface through a prism that is commonly configured in Kretchmann-Raether total internal reflection setup [2]. Furthermore, the setup is fine-tuned by varying either the wavelength of p-polarized light or its incident angle to achieve the resonance condition. This is characterized by (i) a drop in the intensity of the reflected light and (ii) a sharp phase transition; both are located at the resonance position. These two features produce characteristic resonance curves with a resonance position that is sensitive to the properties of the interface. They provide a sensitive method for probing the interfacial processes within ~100 nm of the surface. The measured signal is obtained by (i) tracking the resonance angle [3], (ii) the resonance wavelength [4] or (iii) monitoring the amplitude [5] or the phase [6–8] of the reflected light at the incident angle of the highest gradient. These detection methods feature different sensivities to refractive index change: sensitivity is defined, in this study, as the minimum detectable refractive index change. For instance, phase systems typically demonstrate a higher sensitivity (down to 10^{-8} Refractive Index Units—RIUs), but usually require complex optical system design and do not usually offer a wide dynamic range [8]. On the other hand, amplitude-based detection systems are relatively simple, but their typical sensitivity is ~10^{-5} to 10^{-6} RIUs. Therefore, there is a need to improve their sensitivity for measuring low molecular weight biomolecules in low concentration biological samples. As a result, the differential-intensity detection (Bi-cell SPR) has been introduced which features high sensitivity (10^{-7} to 10^{-8} RIUs) while using a simple optical configuration [9]. Since then, it has been a popular method in different chemical and biological sensing applications [10–15]. Moreover, similar differential approaches are used to improve the signal-to-noise ratio in a range of SPR systems based on nanohole array

* Corresponding author at: Advanced Optics Group, Faculty of Engineering, University of Nottingham, Nottingham, NG7 2RD, UK.
E-mail address: eexsa46@nottingham.ac.uk (S.A. Abayzeed).

http://dx.doi.org/10.1016/j.snb.2016.05.117

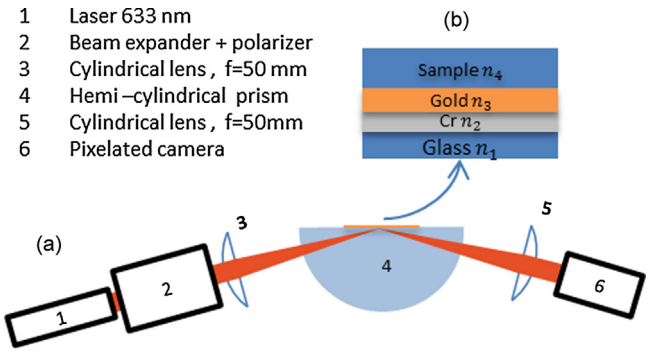

Fig. 1. (a) Surface plasmon resonance sensor: a simplified diagram for a prism-based Kretchmann-Raether configuration which is built to excite surface plasmons at the gold-sample interface using a linearly polarized 633 nm laser beam (b) A Muti-layer model for the sensing structure which is used for simulating the differential—intensity response to change in refractive index and other parameters.

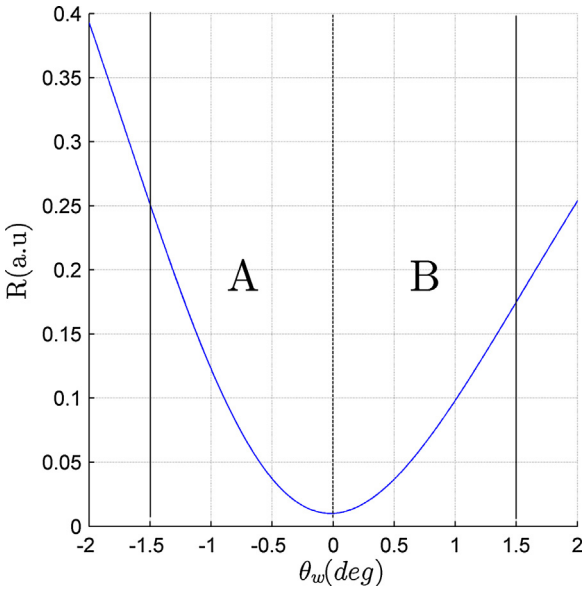

Fig. 2. A window of the SPR curve shows the concept of the Bi-cell detection: the center of the Bi-cell detector (dash-dot line) is aligned to the resonance angle (zero in the graph); solid lines indicate the dimensions of the two units of the detector A and B. The x-axis, normally, represents the angle of the incidence. It has been changed, here, to the angular width by subtracting the angle of incidence from the resonance angle.

technology [16–18]. In addition, the response time of the bi-cell detector is rapid compared to array detectors. This approach is particularly well-suited since our research is directed at resolving weak signals related to dynamic time-resolved processes. In this study, however, we use a pixelated camera to study the method in detail but this will be replaced with a bi-cell detector to perform dynamic measurements.

In this method (which will be called Differential-Intensity Surface Plasmon Resonance (DI-SPR) in this paper), the surface of the metal is illuminated through the prism with a focused beam centered on the resonance angle. The reflected light, which constructs a window of the resonance curve, is detected by a bi-cell photodiode or a pixelated camera as shown in Fig. 1(a). First, by setting the resonance position as the center of the bi-cell detector, the optical power in each half of the curve is detected by one of the units of the detector, as illustrated in Fig. 2. Then, the difference between the two signals is normalized to the total reflected power, proportional to the sum of the two units of the bi-cell detector. This ratio is correlated to the change in the plasmon resonance angle resulting in a three-fold increase in the responsivity compared to the tracking of the resonance position [9]. Also, it has been shown that this method is more sensitive compared to tracking the resonance wavelength [4] or monitoring the intensity of the reflected light at the angle of the highest gradient of the SPR curve [19].

In order to demonstrate how the change in the differential response $\Delta[(A-B)/(A+B)]$ is related to the shift in the resonance angle ($\Delta\theta_0$), the resonance curve is modelled by the following polynomial function

$$R\left(\theta\right) = a_0 + a_1\left(\theta-\theta_0\right) + a_2\left(\theta-\theta_0\right)^2 + a_3\left(\theta-\theta_0\right)^3 + \ldots \quad (1)$$

where θ is the angle of incidence and θ_0 is the resonance angle. Assuming that the SPR curve is symmetric about the resonance angle (θ_0), a quadratic function has previously been used to model the SPR curve [9] using only the second order term $[a_2\left(\theta-\theta_0\right)^2]$ from Eq. (1). The values of A and B are found by integrating the SPR curve using the resonance position (θ_0) and the angular width $\pm\theta_\omega$, corresponding to the width of the unit of the bi-cell detector (Fig. 2), as intergration limits. The integration is repeated, with the same integration limits, after shifting the resonance position by $\Delta\theta_0$[i.e. the second order term becomes $a_2\left(\theta-\theta_0-\Delta\theta_0\right)^2$]. The outputs A and B before and after the resonance shift are used to calculate the change in the differential response $\Delta[(A-B)/(A+B)]$ relative to the shift in the resonance angle ($\Delta\theta_0$)—(Eq. (2)). This relation provides a quick estimate of the responsivity of the differential-intensity system. In this study, responsivity (η) is defined as the obtained differential response per unit shift in resonance angle, assigned a unit of deg^{-1}.

$$\eta = \frac{\Delta\left(\frac{A-B}{A+B}\right)}{\Delta\theta_0} = \frac{3}{\theta_\omega} \quad (2)$$

To arrive at this model, two assumptions were made: (1) the SPR curve R(θ) is symmetric about the resonance angle θ_0; and (2) the sample-induced changes in R will only affect the resonance angle θ_o; without altering the shape of the curve. In reality neither of the assumptions is valid. The model thus estimates the responsivity, taking into consideration the angular width of the excitation beam, however, it does not reflect the effect of the shape of the resonance curve on the responsivity. For this reason, it does not depend on changes in specifications of the sensing structure. As a result, it cannot provide an accurate calibration to calculate the measured change in refractive index in the case of variations in these specifications or evaluate sensitivity enhancement approaches (e.g. replacing gold thin film with a silver thin film). The consequences of the asymmetry of the curve have been studied by Schneider et. al [19]. Also, the model has been modified to accommodate the effect of the measured sample (i.e. the absorbing sample) on the SPR curve and the responsivity [20]. Here, we investigated how the system responds to variations in (i) the properties of the excitation beam such as its angular width and its spatial profile, (ii) the specification of the sensing structure such as the adhesion layer (for example Chromium) and the thickness of the metal film (i.e. Gold) and (iii) the measured sample. As this technique is highly dependent on obtaining high responsivity, the investigation of the effect of these factors is critical. Therefore, this paper aims to provide a detailed evaluation of the responsivity of the differential-intensity surface plasmon resonance sensors using both experimental and theoretical approaches, providing a unified analytical expression for the responsivity. This analysis will also explain the trade-off between the responsivity and the dynamic range and allows users to reconfigure the setup for different experimental settings.

2. System configuration

A differential-intensity surface plasmon resonance sensing platform has been constructed (Fig. 1(a)), adopting a prism-based Kretschmann-Raether configuration. A 633 nm linearly polarized laser is coupled though a prism (BK7, n = 1.515) to the sensor-sample interface. A cylindrical lens is inserted into the beam path so that the light beam is focused to a line onto the sensor chip. Refractive index matching oil (Refractive Index 1.5150) has been used between the prism and the sensor chip to remove undesired reflections from the interfaces. The resonance angle is set to ~72° to excite surface plasmons at the refractive index of distilled water. Since, the incident angle is greater than the critical angle, total internal reflection occurs at the sensor–sample interface. The reflected light is collimated using a second cylindrical lens and detected using a CMOS camera (μEye, IDS GmbH). The angle of convergence of the light beam, inside the prism, is ~ ±3°.

3. Responsivity modelling

The responsivity of the DI-SPR has been modelled through the following steps:

(i) The resonance curve is generated using Fresnel equations [21,2] for the multilayer presented in Fig. 1(b). Also, the quadratic approximation of a narrow range (±1°) of the resonance curve has been used to study the effect of the asymmetry as in Section 5.4. The advantage of the Fresnel model is its realistic representation of the resonance curve with no assumptions, in contrast to the quadratic approximation.
(ii) For each generated curve, the outputs of the bi-cell detector (i.e. A and B) are calculated by the numerical integration of the resonance curve using the angular width as an integration limit. These outputs are used to calculate the differential response $(A-B)/(A+B)$.
(iii) The resonance angle (i.e. the location of the minimum of the curve θ_0) is calculated, by fitting a narrow range of the resonance curve (±1°) to quadratic function, interpolating to the increase accuracy of finding the location of the minimum.
(iv) The responsivity η is the ratio of the change in the differential response to the change in the resonance angle ($\Delta\theta_0$) (Eq. (2)).
(v) The previous steps are repeated with different input parameters (such as the angular width of the excitation beam, the beam profile, thickness of the chromium layer, the thickness of the gold film and the refractive index of the sample).

The effect of the illumination profile is included in the Fresnel model by simulating the beam profile for a specific experimental setup. The beam profile, in one dimension, is given by the Gaussian function (Eq. (3))

$$r = \exp\left(\frac{-x^2}{2(\sigma M)^2}\right) \quad (3)$$

where x is the distance from the center of the bell-shaped curve in mm, σ is the standard deviation which is calculated from the specifications of the laser and M is the magnification of the beam. The simulations considered a beam diameter of 5.1 mm (i.e. the value of σM), matching the specification of the experimental setup.

4. Experiments

The system, described in Fig. 1, has been used to perform the following experiments using sensor chips which were prepared by sputtering approximately 50 nm of gold on a glass slide without the use of the chromium adhesion-promoting layer. For these experiments, refractive index solutions have been prepared using different concentrations of sodium chloride (sigma Bioxtra 99.5%). These solutions have been used to measure the system response to change in refractive index of the sample. For this purpose, a flow cell (with a 57 μl channel) has been mounted on the prism. The response of the system was recorded using the camera while switching the sample in the channel (distilled water n = 1.3319 at 633 nm and 20 °C) to another one with a different refractive index (1.3334). Using these recorded video frames, the resonance curve has been produced for each frame using a pixel-angle calibration. In order to calculate the responsivity as a function of the angular width (Fig. 3), a virtual differential detection approach (i.e. calculating A, B, (A − B)/(A + B) as described in Section 3) has been implemented by the following two steps.

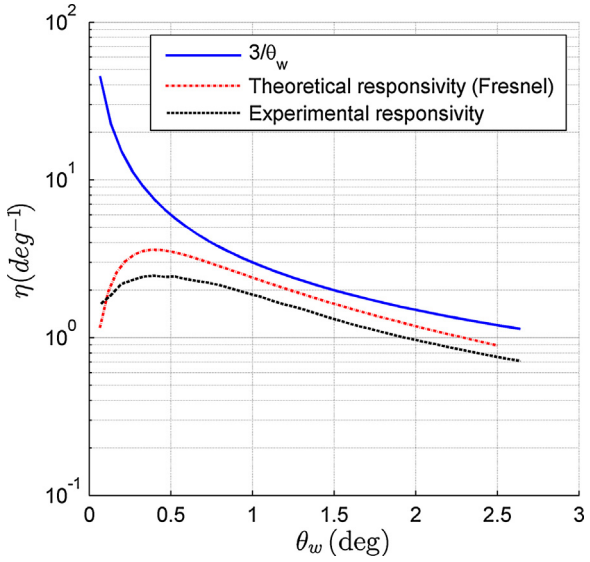

Fig. 3. Theoretical vs Experimental responsivity of DI-SPR. The (blue solid line) presents the theoretical responsivity using $3/\theta_\omega$ model, the (red dotted line) depicts the theoretical responsivity obtained from the Fresnel model for glass slides coated with bare gold, the (black dotted line) experimental responsivity for the bare gold. (For interpretation of the references to color in this figure legend, the reader is referred to the web version of this article.)

(i) Tracking the minimum of the SPR curve to calculate the resonance angle corresponding to the two refractive indices and then the resonance shift ($\Delta\theta_0$).
(ii) Calculating the differential response for different values of the angular widths of the incident beam which are calculated using a pixel-angle calibration.

This analysis provides the means for calculating the responsivity (η) of the DI-SPR using the system response to changes in the resonance angle or the refractive index.

To study the change in responsivity as the resonance position of the SPR curve changes, the refractive index of the sample was stepped from 1.3319 to 1.3409 in increments of 0.5 mRIUs. Similar to the first experiment, the response of the system was recorded using the pixelated camera. The resulting shift in resonance position and the differential response were obtained using the minimum tracking and the virtual differential detection as described above. This experiment explored, in addition to the responsivity, the dynamic range of the system for set of angular widths as discussed later in Section 5.4.

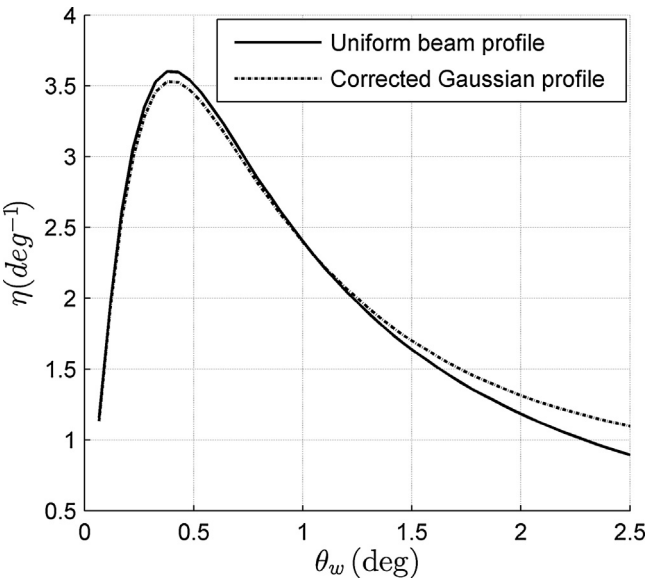

Fig. 4. The responsivity of an ideal uniform beam profile (solid line) and the non-uniform beam profile (dotted line), which is corrected by magnification and spatial filtering.

5. Results and discussions

5.1. Experimental responsivity

As described in the previous section, the responsivity has been calculated experimentally for the sensing structure described in Section 4. Fig. 3 shows the experimental responsivity as a function of the angular width compared to (i) the theoretical responsivity, obtained using the Fresnel model for 50 nm gold when no adhesion layer is undercoated and (ii) the responsivity from the approximated model of ref 8 ($\eta = 3/\theta_\omega$) —(Eq. (2)). A couple of observations can be made from this figure: (i) at small angular width, the theoretical response does not approach infinity as predicted by the model of ref 8 (Eq. (2)), but converges to zero. This is also supported by the experimental results in Fig. 3, (ii) there is a discrepancy between the theoretical and the experimental responsivity which is seen as a reduction in the experimental responsivity with a shift in its maximum. These results are explained later by studying how the system behaves with the variations in the specifications of the sensing structure in Fig. 1(b) starting with the undercoated chromium layer which is commonly used then the effect of the gold thickness and finally the effect of the measured sample. The Fresnel model will be used, with different input parameters, to understand the effect of the above factors. This approach, ultimately, provides a better control in the investigation of their effects.

5.2. The effect of the beam profile

We investigated the effect of the spatial profile of the excitation beam on the responsivity. In Fig. 4, the solid line represents a uniform illumination profile whereas the dotted line represents a Gaussian profile with a diameter that is magnified to 5.1 mm at the input lens. It is clear from the figure that when the beam diameter is magnified, the Gaussian distribution produces a response similar to the uniform illumination, as one would expect. However, some discrepancy is observed for wider angular ranges due to the increase of the Gaussian effect. The theoretical results presented in the rest of the paper assume a uniform distribution.

5.3. The influence of the specifications of the sensing structure

First, since the chromium adhesion layer is commonly-used, we address its effect on the responsivity. This is performed by calculating the responsivity for a set of thicknesses, from 0 nm to 3 nm, of this layer. One important effect of the Cr layer is that, for any angular width, there is a reduction in the responsivity as the thickness of the Cr layer increases. This is shown clearly in Fig. 5(a). It is also observed that the angular width of the peak responsivity shifts to the right with increasing Cr thickness. In order to explain these results, we looked at the effect of the Cr layer on the SPR curve, which is shown in Fig. 5(b), and more specifically, the FWHM and the minimum reflectivity of the curve (it will be called a_0 in this text), in Fig. 5(c) and (d), respectively. As the thickness of Cr increases, both the FWHM and a_0 increases.

Second, we investigated the effect of the gold layer. The responsivity of the differential technique has also demonstrated a noticeable dependence on the thickness of the gold film. Fig. 6(a) shows results obtained by changing the thickness of Au, without any undercoated Chromium layer. Peak responsivity is obtained, for all angular widths, at gold thickness around 48 nm, which decreases rapidly either side of the peak. Fig. 6 (a) can be explained by considering the SPR curve in Fig. 6(b), and its parameters: FWHM and a_0 in Fig. 6(c) and (d), respectively. Although the FWHM decreases with increasing Au thickness, the a_0 response shows a turning point at 47 nm, which correlates with the responsivity in 6(a).

A close look into Figs. 5 and 6 reveals that the minimum reflectivity a_0 of the SPR curve is strongly related to the responsivity, showing a negative correlation. For instance, a deeper SPR curve, which is noticed around the thickness of 48 nm, demonstrates a higher responsivity. Similarly, as the thickness of the adhesion layer increases, the minimum reflectivity becomes higher and so the responsivity decreases. By getting back to theoretical estimation of the responsivity, the above observations could be related to the zero order of the polynomial that represents the SPR curve. This zero order is not included in the model presented by Eq. (2) and so it does not include the observations in Figs. 3, 5(a) and 6(a).

5.4. The effect of the sample and the asymmetry of the SPR curve

The effect of the measured sample on the responsivity has been investigated. SPR curves were produced using the Fresnel model (i.e. asymmetric curves) and also a second order approximation of the SPR curve, with the zero order a_0 included (i.e. symmetric curves). The zero order of the function has not been ignored, as Figs. 5 and 6(d) suggest a strong link between a_0 and the system response, which will be discussed in more detail in Section 5.5.

As seen from both the second-order approximation and the Fresnel model (see Fig. 7(a) and (b), respectively), the responsivity drops when there is a change in the refractive index of the sample (expressed in the corresponding resonance shift—$\Delta\theta_0$). However, the Fresnel model demonstrated the information regarding the asymmetry of the curve about the resonance angle. As seen in Fig. 7(b), the maximum responsivity is shifted to the left and it is not located at the origin (i.e. the initial resonance angle) in contrast to the quadratic case—Fig. 7(a). As the maximum responsivity is obtained where the bi-cell detector is balanced, this shift is rectified by mechanical translation of the detector so that the condition $(A - B)/(A + B)$ equal to zero is satisfied. However, if a linear array detector [22] or a CCD [4] is used, the offset can be calculated and transformed to the corresponding number of pixels.

This analysis also presents valuable information about the trade-off between the responsivity and the dynamic range (Fig. 7). For any angular width, the dynamic range could be defined with reference to the drop of the responsivity from its maximum value. Therefore, as in Fig. 8, two definitions of the dynamic range can used; the

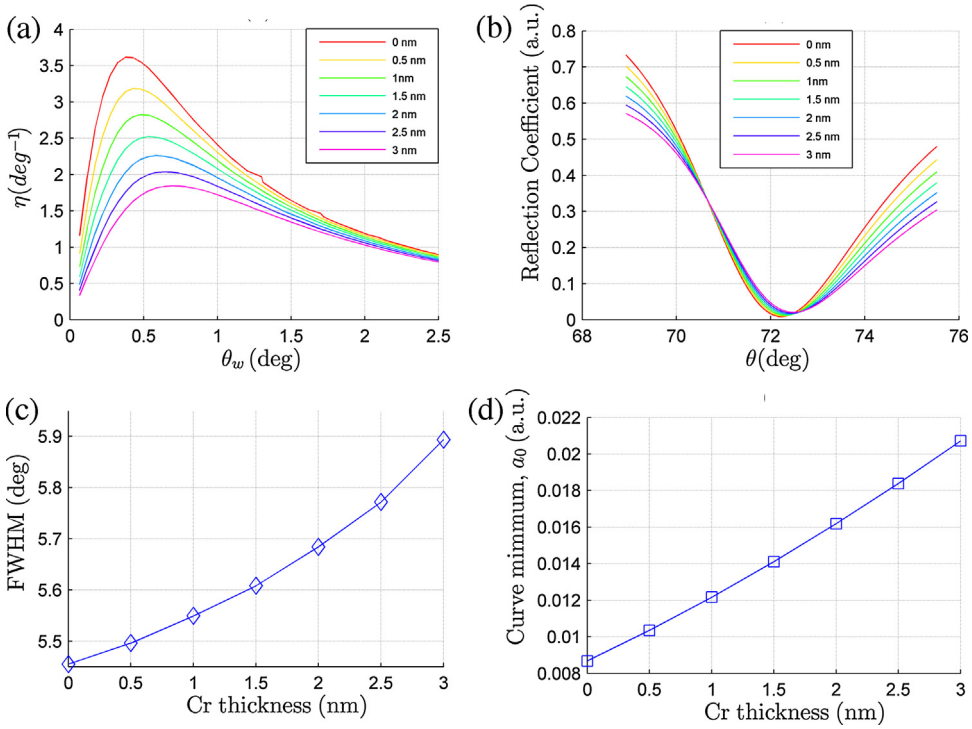

Fig. 5. The effect of the adhesion layer on the responsivity of the DI-SPR. (a) The effect of the thickness on the angular width dependence of the responsivity. (b) The effect of the thickness of the adhesion layer on the SPR curve. Curve parameters: (c) FWHM of the curve and (d) Reflectivity at the minimum of the curve.

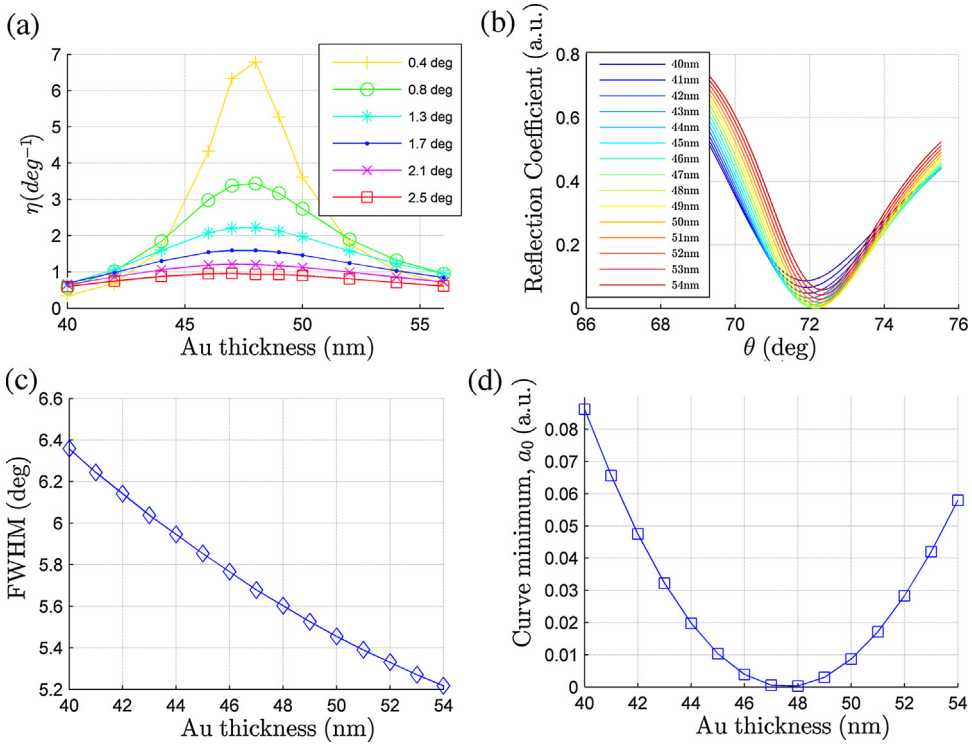

Fig. 6. The effect of the metal thickness on the responsivity of the DI-SPR. (a) The angular width dependent responsivity. (b) The effect of the metal thickness on the SPR curve. Curve parameters: (c) FWHM of the curve and (d) Reflectivity at the minimum of the curve.

change in the resonance position where the responsivity drops to 95% or 50% of the peak value. A similar trade-off is also observed by changing the value of the angular width. This is only observed for the case of angular width greater than 0.4^0. In this range, the dynamic range increases as the angular width increases but the responsivity is reduced; see Fig. 8(a) and (b). However, for angular widths smaller than 0.4^0 neither responsivity nor dynamic range is improved. This flexibility, which is offered by the angular width, is valuable for experimental design. For example, to measure a low concentration sample, the design of the experiment favours the

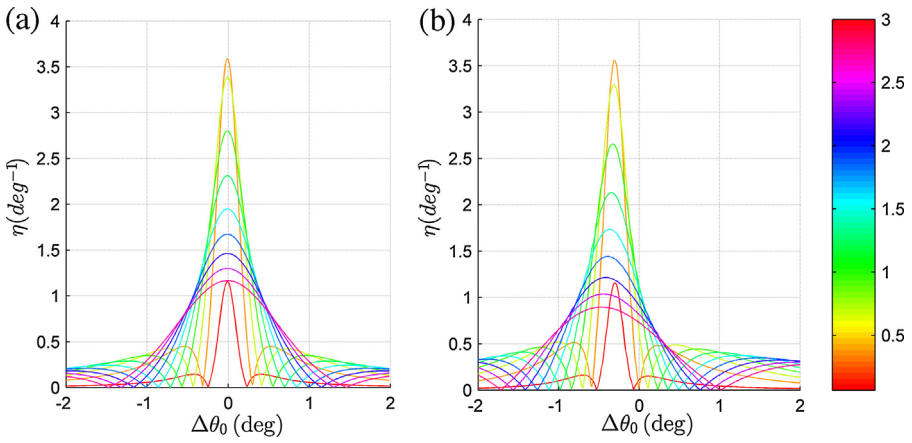

Fig. 7. The drop in the responsivity as a function of the SPR shift from its initial position, presenting a comparison between (a) the quadratic approximation of the resonance curve and (b) numerical simulation using a one dimensional, multi-layer model of the sensing structure. The colormap refers to different angular widths.

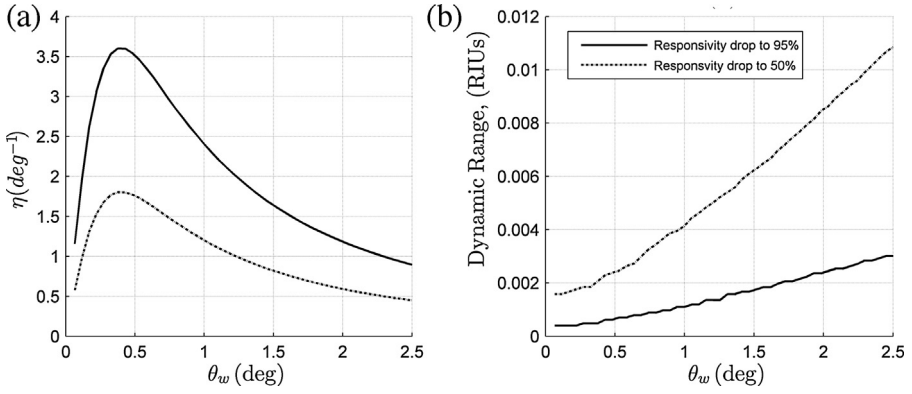

Fig. 8. Theoretical demonstration of a trade-off between (a) the responsivity and (b) the dynamic range as controlled by the selection of the angular widths of the excitation beam. The dynamic range can be defined in relation to the drop off in the responsivity: responsivity drops to 95% of the peak (solid line) or 50% of the peak (dotted line).

sensitivity over the dynamic range and therefore a small value of the angular width is selected and vice versa. The drop in responsivity, as SPR curve shifts (Fig. 7), is due to the use of a fixed reference point for the differential detection (i.e. the initial resonance angle) while the resonance position shift in response to the change in refractive index. So, increasing the dynamic range by moving the reference using a pixelated detector has been suggested elsewhere [22].

The drop of the responsivity, due to changing the refractive index of the sample, has also been measured experimentally. From this experiment, shifts of the resonance position ($\Delta\theta_o$) are determined for the corresponding changes in refractive index and compared to the response of the DI-SPR (A − B)/(A + B), as depicted in Fig. 9. Responsivity, as defined earlier, is found from the change of the DI-SPR response divided by the resonance shift ($\Delta\theta_o$). The experimental responsivity of the system, as a function of the resonance shift, is presented in Fig. 10. This graph is calculated from the gradient of the DI-SPR response in Fig. 9 after smoothing by spline interpolation. From Fig. 10, it is noticed that responsivity increases as angular width increases with a peak at ∼0.5° before it drops again, similar to the theoretical results of Figs. 3, 7(b) and 8(a). The dynamic range increases with the angular width confirming the previous theoretical observations (see Fig. 7 and 8(b)).

For all the angular widths, the experimental responsivity is lower compared to the theoretical one presented in Fig. 7(b). The causes of this drop are investigated by looking at the effect of the thickness of the gold thin film. It is found that the experimental SPR curve matches the theoretical curve of a thin film thickness of 45 nm with no undercoat, see Fig. 11-inset. Similarly, the experimental responsivity of the system agrees with the theoretical responsivity that generated from Fresnel model for 45 nm of gold thin film with no undercoat. The results in Fig. 11, is further confirmed by comparing the theoretical and the experimental minimum reflectivity and the full-width-half-maximum (FWHM). The experimental FWHM, for 45 nm of gold thin film, is 5.87° compared to the theoretical value of 5.85° (see Fig. 6(c)). Also, the experimental minimum reflectivity, is 0.018 compared to the theoretical figure of 0.0102 (see Fig. 6(d)). The agreement of these parameters confirms the previous statement that responsivity varies with the minimum reflectivity and the FWHM of the curve. It is noticed that there is a ∼0.3° difference between the location of the maximum in case of the experimental responsivity in Fig. 11 compared to the theoretical one in Fig. 7(b). This discrepancy is attributed to the reflectivity fluctuations of the experimental SPR curve. In practice, the maximum responsivity is obtained by balancing the bi-cell detector or finding the reference pixel in the case of using array detectors as stated previously, so the shift does not affect the operation of the instrument.

5.5. Modifications to the responsivity model

The responsivity of DI-SPR depends, not only on the angular width of the excitation beam, but also on the other parameters of the SPR curve (Figs. 5 and 6(d)). Since the performance of the DI-SPR is strongly dependent on obtaining high responsivity, there is a need to develop a theoretical framework that encounters for the effect of these factors. In order to translate their effect in an analytical expression, the responsivity is derived using a second-order

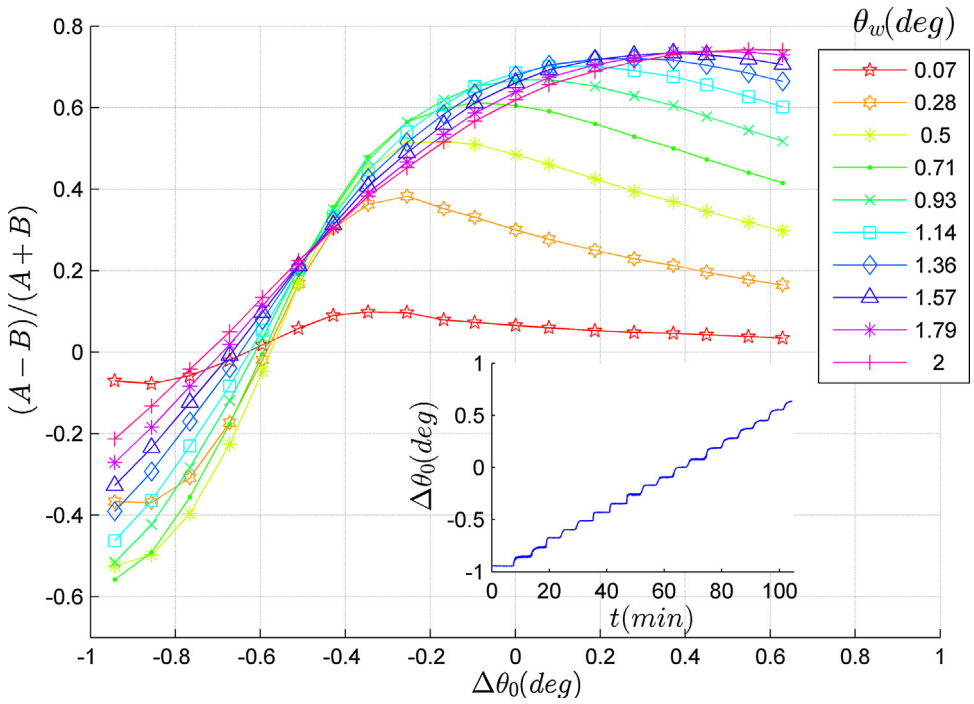

Fig. 9. The response of the DI-SPR due to the shift of the resonance position. The response is measured for a set of angular widths. The inset shows real time tracking of the resonance position while the refractive index is changed.

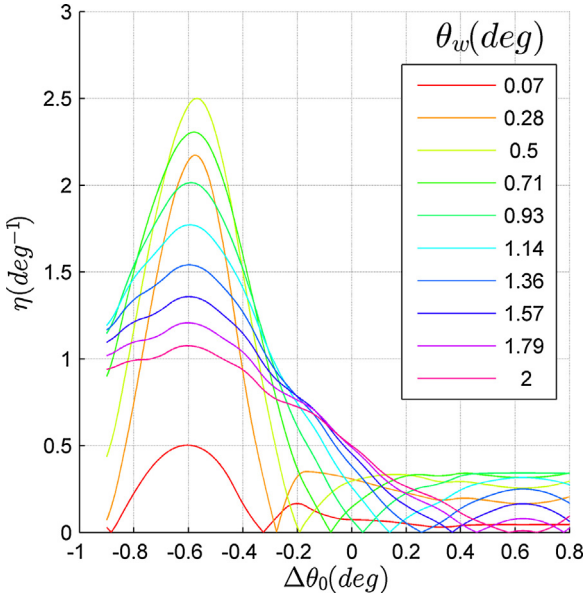

Fig. 10. Experimental responsivity (η) drops as the resonance position (θ_o) shifts which is presented for a set of angular widths of the excitation beam, obtained from the gradient of the curve fitted to data in Fig. 9.

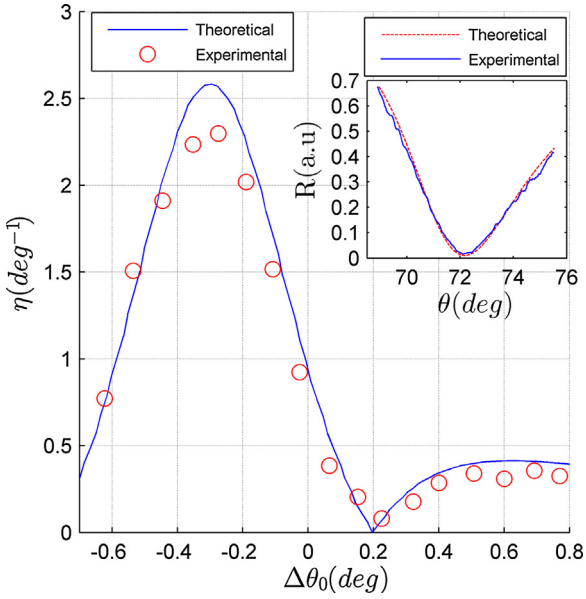

Fig. 11. A comparison between the experimental and the theoretical responsivity for an angular range of 0.5°. The two graphs are overlaid for the purpose of comparison. The inset present the corresponding experimental and the theoretical SPR curves. Both SPR and responsivity curves are calculated for Au thickness of 45 nm using Fresnel models. The experimental SPR curve is generated by subtracting the dark current and normalising to the total internal reflection.

polynomial representation of the SPR curve including the zero order and the second order terms from Eq. (1). Eq. (4) gives the responsivity (η) obtained from the second order polynomial, with the a's being the coefficients of the power series that represents the SPR curve. For 50 nm gold, $a_0 = 0.008$ and $a_2 = 0.14$.

$$\eta = \frac{3a_2\theta_\omega}{3a_0 + a_2\theta_\omega^2} \tag{4}$$

Eq. (4) is validated against the data generated from the Fresnel model as presented in Fig. 12. As seen in Fig. 12, Eq. (4) reproduces the responsivity of Fresnel model, but it departs at large values of the angular width, reflecting the effect of the asymmetry of the SPR curve. More accurate representation of the responsivity is achieved by fitting Eq. (5) to the responsivity data that is generated from the Fresnel model in Fig. 12. For 50 nm gold, $b_0 = 0.011$ b_2=0.2 and b_3=0.03.

$$\eta = \frac{3b_2\theta_\omega + b_3\theta_\omega^2}{3b_0 + b_2\theta_\omega^2 + b_3\theta_\omega^3} \tag{5}$$

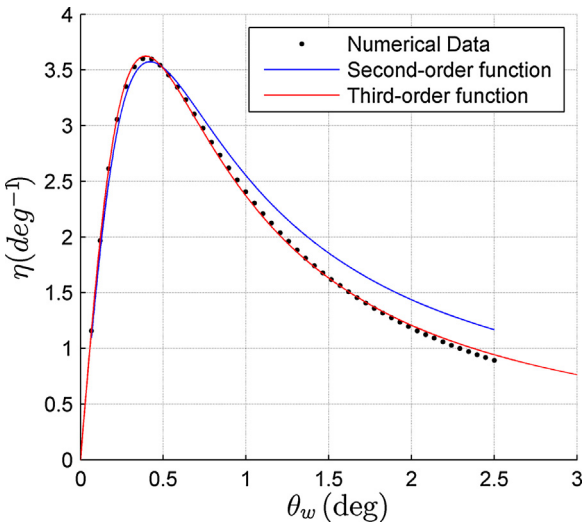

Fig. 12. Comparison between the second-order and third-order models. Numerically generated data is fitted to the third-order function (red) and compared to the second order function (blue) which is obtained from the polynomial model of the SPR curve. (For interpretation of the references to color in this figure legend, the reader is referred to the web version of this article.)

These two mathematical representations account for the variation of the thickness of the noble metal (e.g. Silver or gold), the spatial profile of the laser beam and the metallic adhesion layer as reflected in the values of the coefficients. They both can be reduced to Eq. (2) under the condition ($\lim_{a_0\to 0}\eta$ and $\lim_{(b_0,b_3)\to(0,0)}\eta$ respectively). Moreover, both expressions (Eqs. (4) and (5)) account for the effect of the angular width and explain the drop of the responsivity at smaller angles. This drop is due to the inclusion of the second order and the zero order of the polynomial to Eq. (2). Both coefficients are valuable measures for the properties of the SPR curve. The former reveals information on the gradient of the curve. The latter represents the minimum reflectivity, which cannot be ignored for smaller angular widths (see the denominator of Eq. (4)). These coefficients are used to estimate the point of maximum responsivity, as given by the term $\left(\theta_\omega = \sqrt{3a_0/a_2}\right)$, which can be obtained by differentiating Eq. (4). This term also explains how the maximum translates with the change in the SPR curve (e.g. the shift in the maximum responsivity of the theoretical and the experimental curves in Fig. 3 and the use of Cr undercoat in Fig. 5(a)). Moreover, including these two factors makes a unified model, which could be extended to consider the measurement of samples that changes the characteristics of the curve (i.e. has absorption properties, [20]). Prior information on how the experiment changes the SPR curve, in addition to the angular shift, helps selecting the operating point that optimises the sensitivity and the dynamic range.

6. Conclusions

Previous studies of the responsivity of the DI-SPR did not consider the effect of the parameters of the SPR curve. In this paper, we have presented a modified model that considers the influence of the noble metal thickness, the adhesion layer, and the inhomogeneity of the illumination profile, as reflected in the parameters of the SPR curve. The model can be used to calibrate the DI-SPR systems directly from coefficients of SPR curves, with no need to perform refractive index stepping. We also evaluated, both theoretically and experimentally, the dependence of the system performance on the angular width of the excitation beam in addition to the bi-cell detector balance. These findings shed the light on the selection of the angular width for a tradeoff between the responsivity and the dynamic range. For example, measuring transparent samples that induce only a shift in the resonance curve, the angular width is selected for the maximum responsivity if the measured refractive index change is very small (i.e. narrow dynamic range). In contrast, a wider angular window is selected when a wide dynamic range is needed.

In future, the model could be used to recommend an optimal operating point when measuring samples with absorption properties (i.e. Changing the shape of the SPR curve), by using prior information about the sample to predict the coefficients of the model (or the SPR curve). This framework can also be used to evaluate strategies of improving the sensitivity, by using a more efficient plasmonic sensor (e.g. the use of silver or silver–gold bi-layers).

Acknowledgements

The authors acknowledge the support of Engineering and Physical Sciences Research Council (EPSRC) for a platform grant 'Strategies for Optimal Biological Imaging' (Ref: EP/G005184/1).

References

[1] J. Homola, S.S. Yee, G. Gauglitz, Surface plasmon resonance sensors: review, Sens. Actuators B Chem. 54 (January (1–2)) (1999) 3–15.
[2] Surface Plasmons on Smooth and Rough Surfaces and on Gratings, vol. 111, Springer, Berlin Heidelberg, 1988.
[3] S. Owega, D. Poitras, Local similarity matching algorithm for determining SPR angle in surface plasmon resonance sensors, Sens. Actuators B Chem. 123 (April (1)) (2007) 35–41.
[4] O.R. Bolduc, L.S. Live, J.-F. Masson, High-resolution surface plasmon resonance sensors based on a dove prism, Talanta 77 (March (5)) (2009) 1680–1687.
[5] C. Pettit, K. Assiongbon, J. Garland, D. Roy, Time resolved detection of electrochemical effects by surface plasmon resonance measurements: a simple technique using a large area single cell photodiode, Sens. Actuators B Chem. 96 (November (1–2)) (2003) 105–113.
[6] S.Y. Wu, H.P. Ho, W.C. Law, C. Lin, S.K. Kong, Highly sensitive differential phase-sensitive surface plasmon resonancebiosensor based on the Mach–Zehnder configuration, Opt. Lett. 29 (October (20)) (2004) 2378–2380.
[7] I.R. Hooper, J.R. Sambles, M.C. Pitter, M.G. Somekh, Phase sensitive array detection with polarisation modulated differential sensing, Sens. Actuators B Chem. 119 (December (2)) (2006) 651–655.
[8] J. Wang, R.J. Smith, R.A. Light, J.L. Richens, J. Zhang, P. O'shea, C. See, M.G. Somekh, Highly sensitive multipoint real-time kinetic detection of Surface Plasmon bioanalytes with custom CMOS cameras, Biosens. Bioelectron. 58 (August (100)) (2014) 157–164.
[9] N.J. Tao, S. Boussaad, W.L. Huang, R.A. Arechabaleta, J. D'Agnese, High resolution surface plasmon resonance spectroscopy, Rev. Sci. Instrum. 70 (December (12)) (1999) 4656–4660.
[10] E. Forzani, H. Zhang, W. Chen, N. Tao, Detection of heavy metal ions in drinking water using a high-resolution differential surface plasmon resonance sensor, Environ. Sci. Technol. 39 (March (5)) (2005) 1257–1262.
[11] R.J. Mani, R.G. Dye, T.A. Snider, S. Wang, K.D. Clinkenbeard, Bi-cell surface plasmon resonance detection of aptamer mediated thrombin capture in serum, Biosens. Bioelectron. 26 (August (12)) (2011) 4832–4836.
[12] J. Xiang, J. Guo, F. Zhou, Scanning electrochemical microscopy combined with surface plasmon resonance: studies of localized film thickness variations and molecular conformation changes, Anal. Chem. 78 (March (5)) (2006) 1418–1424.
[13] F. Song, F. Zhou, J. Wang, N. Tao, J. Lin, R. Vellanoweth, Y. Morquecho, J. Wheeler-Laidman, Detection of oligonucleotide hybridization at femtomolar level and sequence-specific gene analysis of the Arabidopsis thaliana leaf extract with an ultrasensitive surface plasmon resonance spectrometer, Nucleic Acids Res. 30 (July (14)) (2002).
[14] R. Wang, A. Lajevardi-Khosh, S. Choi, J. Chae, Regenerative Surface Plasmon Resonance (SPR) biosensor: real-time measurement of fibrinogen in undiluted human serum using the competitive adsorption of proteins, Biosens. Bioelectron. 28 (October (1)) (2011) 304–307.
[15] X. Yao, X. Li, F. Toledo, C. Zurita-Lopez, M. Gutova, J. Momand, F. Zhou, Sub-attomole oligonucleotide and p53 cDNA determinations via a high-resolution surface plasmon resonance combined with oligonucleotide-capped gold nanoparticle signal amplification, Anal. Biochem. 354 (July (2)) (2006) 220–228.
[16] A.-P. Blanchard-Dionne, L. Guyot, S. Patskovsky, R. Gordon, M. Meunier, Intensity based surface plasmon resonance sensor using a nanohole rectangular array, Opt. Express 19 (August (16)) (2011) 15041.
[17] C. Escobedo, S. Vincent, A.I.K. Choudhury, J. Campbell, A.G. Brolo, D. Sinton, R. Gordon, Integrated nanohole array surface plasmon resonance sensing device using a dual-wavelength source, J. Micromech. Microeng. 21 (11) (2011) 115001.

[18] M. Das, D. Hohertz, R. Nirwan, A.G. Brolo, K.L. Kavanagh, R. Gordon, Improved performance of nanohole surface plasmon resonance sensors by the integrated response method, IEEE Photonics J. 3 (June (3)) (2011) 441–449.
[19] M. Schneider, A. Andersen, P. Koelsch, H. Motschmann, Following fast adsorption processes with surface plasmon spectroscopy: reflectivity versus mismatch tracking, Sens. Actuators B Chem. 104 (January (2)) (2005) 276–281.
[20] J. Garland, K. Assiongbon, C. Pettit, D. Roy, Surface plasmon resonance transients at an electrochemical interface: time resolved measurements using a bicell photodiode, Anal. Chim. Acta 475 (January (1–2)) (2003) 47–58.
[21] M. Born, E. Wolf, Chapter 1-Basic properties of the electromagnetic field, in: M.B. Wolf (Ed.), Principles of Optics, Pergamon, 1980, pp. 1–70 (Sixth (Corrected) Edition).
[22] J. Rhee, D. Wang, N. Tao, Y. Joo, CMOS image sensor array for surface plasmon resonance spectroscopy, in: Proc. SPIE Volume 5301, Sensors and Camera Systems for Scientific, Industrial, and Digital Photography Applications V, 34 (June 7, 2004).

Biographies

Sidahmed Abayzeed received BEng (Hons) in Biomedical Engineering from Sudan University of Science and Technology, Khartoum, Sudan. He obtained MSc in Bioengineering and PhD in Electrical and Electronic Engineering from the University of Nottingham, UK. He is currently a postdoctoral researcher with interest in developing label-free technology for functional imaging of living cells.

Richard Smith completed his MEng in electronic and electrical engineering in 2002, and went on to obtain an PhD on combining optical microscopy and signal processing techniques to expand the measurement capabilities of optical microscopes in 2006, both from the University of Nottingham. He is currently a senior research fellow at the University of Nottingham, with research interests in plasmonics, and nano structures/devices for use in high frequency laser ultrasonics.

Kevin Webb completed his first degree in Biomedical Science and a PhD in Physiology at the University of Auckland, New Zealand. Since that time his work has combined functional imaging and electrophysiology to the study of living cells and tissue systems. He is presently Assistant Professor of Applied Optics at the University of Nottingham and his main research interests are in real-time and high-resolution measurements of physiology in the transparent tissues of the eye.

Prof. Michael Geoffrey Somekh Mike Somekh took his first degree from Oxford University in Metallurgy and Materials Science. He then completed his PhD in Microwave Electronics from Department of Physics, University of Lancaster in 1981. He then returned to Oxford to work on contrast mechanisms in Acoustic Microscopy first as a research associate then as an EPSRC Research Fellow. He then joined University College London as lecturer and Director of the Wolfson Unit for micro-NDE. In 1989 he joined the University of Nottingham as Senior Lecturer and was promoted to Reader (1992) and Professor of Optical Engineering (1994). His research interests are novel microscopy, imaging sensors and laser ultrasonics. He is Chair Professor in Biophotonics at Hong Kong Polytechnic University. Mike was elected to the Royal Academy of Engineering (the UK engineering Academy) in 2012 in recognition of his interdisciplinary work. In addition to his post at PolyU he is an honorary professor at the University of Nottingham and Zhejiang University, Hangzhou.

Dr Chung Wah See graduated in Electronic and Electrical Engineering from University College London in 1981, and received his PhD in 1986, also from UCL. His PhD and Post-Doctoral research concerned high resolution, ultra-sensitive optical systems for imaging and metrology. From 1988 to 1992, CWS worked as a Senior Research Engineer at Rank Taylor Hobson Ltd, Leicester. His primary responsibility was to develop various optical metrology systems for texture, and form measurements. CWS joined the School of Electrical and Electronic Engineering, University of Nottingham in October 1992 as a Lecturer, and was appointed a Senior Lecturer in 2001. His research interests concern optical imaging systems, including super-resolution techniques and ultra-sensitive imaging using surface plasmon resonance.